Biosensors and Bioelectronics 169 (2020) 112555

Contents lists available at ScienceDirect

Biosensors and Bioelectronics

journal homepage: http://www.elsevier.com/locate/bios

Numerous long single-stranded DNAs produced by dual amplification reactions for electrochemical detection of exosomal microRNAs

Liang-Liang Wang [a,b], Wen-Qian Chen [a,b], Yu-Ru Wang [a,b], Lu-Peng Zeng [a,b], Ting-Ting Chen [a,b], Guan-Yu Chen [a,b], Jing-Hua Chen [a,b,*]

[a] Department of Pharmaceutical Analysis, The School of Pharmacy, Fujian Medical University, Fuzhou, Fujian Province, 350122, PR China
[b] Fujian Key Laboratory of Drug Target Discovery and Structural and Functional Research, The School of Pharmacy, Fujian Medical University, Fuzhou, Fujian Province, 350122, PR China

ARTICLE INFO

Keywords:
Long single-stranded DNAs
Electrochemical biosensor
Dual amplification reactions
Exosomal microRNAs
Primer exchange DNA amplification Reaction

ABSTRACT

Exosomal microRNAs (miRNAs) have been explored as an extremely promising biomarker of liquid biopsy for the diagnosis, treatment and prognosis of diseases such as cancer, in which sensitive and selective detection is significant. Herein, we describe the construction and testing of an electrochemical biosensor for the sensitive detection of exosomal miRNAs. It is based on synthetizing numerous long single-stranded DNAs (ssDNAs), which are produced by dual amplification reactions of target-triggered cyclic strand displacement reaction (TCSDR) and primer exchange DNA amplification reaction (PEDAR). In the first signal amplification step, target miRNAs are captured by the hairpin DNA strands (capture probes, Cp) that are immobilized on electrode. After strand unfolding with target capture, primer probes (Pp) enable to hybridize with Cp. And then target miRNAs were displaced for starting the TCSDR process that enable the introduction of numerous primers in Pp. In the second signal amplification step, the primers associated with PEDAR produce copious amounts of elongated ssDNAs. These ssDNAs absorb abundant quantities of methylene blue (MB) that enables the highly sensitive and label-free detection of exosomal miRNAs. This dual amplification process is characterized by a low limit of detection (LOD) of 3.04 aM. In addition, the electrochemical biosensor exhibits good selectivity for miR-21 detection, and shows benefits of simple operation, low cost, portability. Overall, the electrochemical biosensor provides a promising platform for the early diagnosis and screening of tumor biomarkers and the development of devices for point-of-care testing (POCT).

1. Introduction

Advancing the state of art in the early diagnosis, treatment and prognosis of cancers requires discovery and development of new concepts in exosome-based liquid biopsy (Kalluri and LeBleu, 2020; Zhang et al., 2017). Exosomes are extracellular vesicles originating from an endosomal pathway encapsulating molecular cargoes with a lipid bilayer and secreted as a spherical structure held together with a plasma membrane in the diameter range of 40–160 nm (Kalluri and LeBleu, 2020). By delivering their cargoes (e.g., proteins, RNAs) to various recipient cells, exosomes maintain a close association and communication with the intracellular environment that are important in tumor pathology, immune responses, and cardiovascular diseases (Aghebati--Maleki et al., 2019; Boriachek et al., 2018a; Groza et al., 2020; Kalluri and LeBleu, 2020; Wang and Gires, 2019). In particular, exosomal microRNAs (miRNAs), a type of non-coding RNA with a single strand of 18–24 nucleotides, take on specific clinical relevance. The expression level of specific sequences has been useful at identifying occurrence of cancer as well as its development and metastasis (Fong et al., 2015; He et al., 2018; Kulkarni et al., 2019; Yoshii et al., 2019; Zeng et al., 2018). In addition, the abundance and quality of exosomal miRNAs in biofluids are made considerably stable because of the protection that the exosomal lipid bilayer affords against environmental shear stresses and RNase (Jiang et al., 2019). The biological functions of exosomal miRNAs enhanced their therapeutic and diagnostic potential as biomarkers acquired by liquid biopsy (Salehi and Sharifi, 2018). The development of a sensitive and accurate quantification method for exosomal miRNAs is therefore meaningful and urgent.

The most common methods for detection of exosomal miRNAs mainly rely on the reverse transcription-polymerase chain reaction (RT-

* Corresponding author. Department of Pharmaceutical Analysis, The School of Pharmacy, Fujian Medical University, Fuzhou, Fujian Province, 350122, PR China.
E-mail address: cjh_huaxue@126.com (J.-H. Chen).

https://doi.org/10.1016/j.bios.2020.112555
Received 2 July 2020; Received in revised form 19 August 2020; Accepted 24 August 2020
Available online 1 September 2020

PCR) (Zeng et al., 2018), northern blotting (Qu et al., 2016), next generation sequencing (Amorim et al., 2017), and microarray analysis (Valadi et al., 2007). These methods are limited by the complicated and expensive equipment they require, the rigorous operation conditions, and low sensitivity. To sidestep these limitations, some biosensors have been developed with alternate signal transduction elements, such as surface-enhanced Raman scattering (Lee et al., 2019b; Pang et al., 2019), surface plasmon resonance (Zou et al., 2020), fluorescence (Cho et al., 2019; Gao et al., 2019; Lee et al., 2019a; Wang et al., 2019a, Wang et al., 2020a, Wang et al., 2020b; Zhao et al., 2020) and electrochemistry (Boriachek et al., 2018b; Guo et al., 2020; Liu et al., 2019; Luo et al., 2020; Tang et al., 2020; Tavallaie et al., 2018; Zhang et al., 2018). The electrochemical biosensors possess the intrinsic benefits of easy operation, rapid analysis speed, low cost, and high sensitivity (Abolhasan et al., 2019; Choi et al., 2016; Zhao et al., 2015). Further, they have achieved limited success at the sensitive detection of exosomal miRNAs. As the electrochemical equipment trend towards systems integration, miniaturation, automation, and artificial intelligence, electrochemical methods have begun to exhibit significant value for the application of tumor diagnosis (Dai and Liu, 2019). Furthermore, to detect predictive exosomal miRNAs at low and even trace levels, the electrochemical biosensors have introduced additional isothermal nucleic acid amplification strategies. For instance, Tang et al. utilized the toehold mediated strand displacement reaction (TMSDR) to release primer sequences, and hybridize the primers to DNA templets. This led to the generation of multiple copies of exosomal miRNAs using rolling circle amplification (RCA). This combination of target amplification with signal-amplified electrochemical detection produced a limit of detection (LOD) of 2.75 fM (Tang et al., 2020). Zhang et al. designed a bipedal DNA walker based on TMSDR for electrochemical signal amplification. This achieved the sensitive detection of exosomal miRNAs with an even smaller LOD of 67 aM (Zhang et al., 2018). Guo et al. fabricated an ultrasensitive electrochemical biosensor based on the signal amplification from the hybridization chain reaction (HCR), achieving an attomolar level detection limit of 53 aM with reduced false-positive signals (Guo et al., 2020). In general, however, RCA templets are burdened with complicated ligation protocols. The DNA walker-based detection method requires a multi-step protocol and complicated labeling technique. The HCR technique may be restricted to the amplification of double-stranded DNA. Recently, a novel isothermal nucleic acid amplification technique defined as primer exchange reaction have attracted people's attention owing to its automated and programmable one step amplification of arbitrary single-stranded DNA (ssDNA). This technique has been applied for in situ optical imaging and detection of

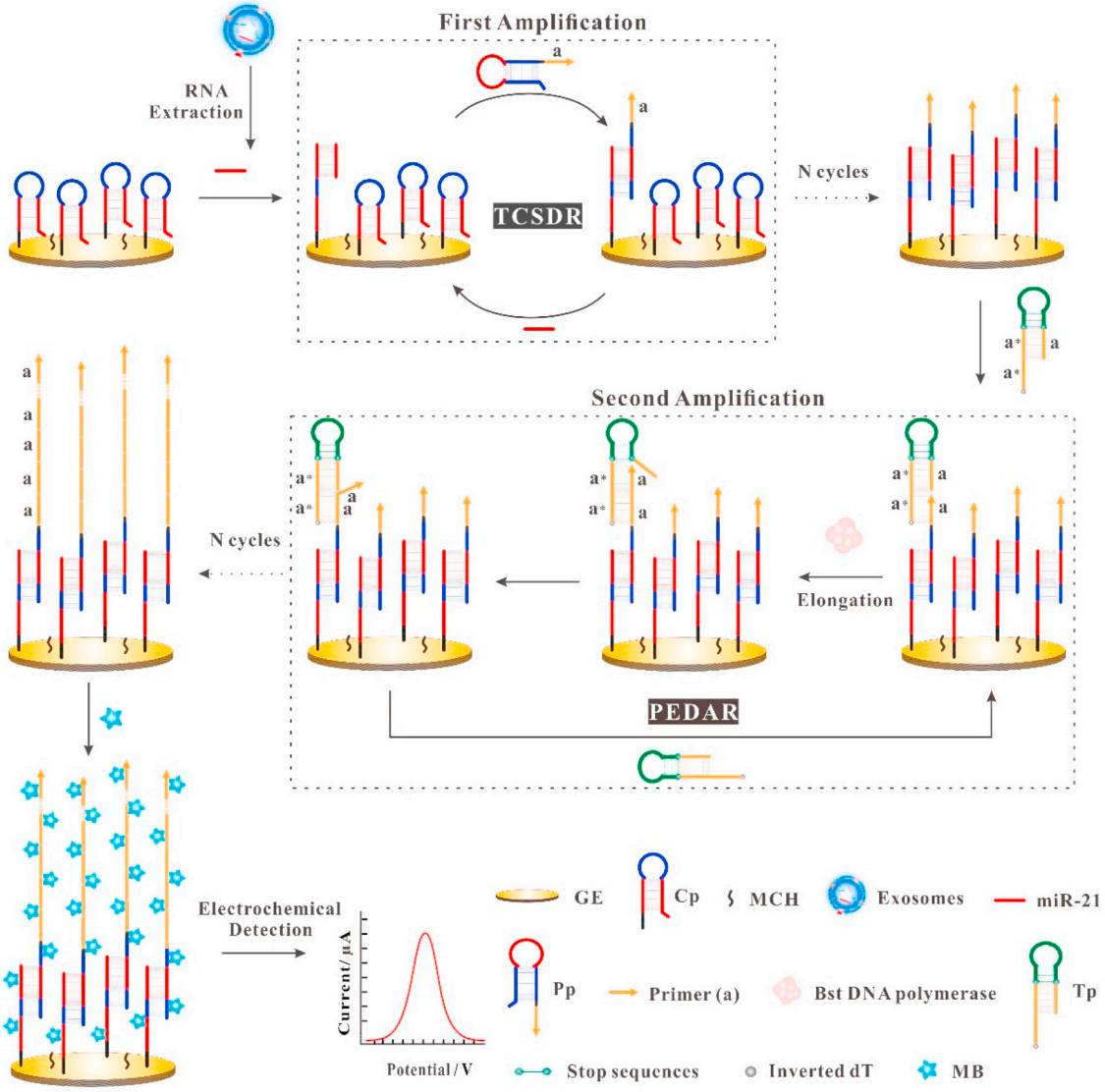

Scheme 1. The principle of the electrochemical biosensor for the detection of exosomal miRNAs.

proteins and nucleic acid in cells (Kishi et al., 2018, 2019; Saka et al., 2019). Additional efforts to exploit the full advantages of this technique by combining this technique with other detection modalities (e.g., electrochemistry) are being considered.

Inspired by the above studies, we developed a miRNAs electrochemical biosensor coupling of numerous long ssDNAs products that are produced by the dual amplification reactions of target-mediated cyclic strand displacement reaction (TCSDR) and primer exchange DNA amplification reaction (PEDAR). Exosomal miR-21, a common biomarker of breast cancer (Hannafon et al., 2016), was selected as the target marker to evaluate detection performance. As shown in Scheme 1, miR-21 initiates the first round of amplification of TCSDR fueled by the presence of primer probes (Pp). After cycling a large number of times, TCSDR introduces a copious set of primers. Thereafter, templet probes (Tp) hybridize with the exposed primers. The second PEDAR signal amplification protocol is implemented with the assistance of Bst DNA polymerase and produces numerous long ssDNAs. Ultimately, redox molecule, methylene blue (MB), is used to generate an electrochemical signal, as it binds to ssDNA by electrostatic adsorption, or double stranded DNA by π-π stacking interactions (Hou et al., 2015; Pan et al., 2007). In theory, after undergoing the dual amplification reactions, a trace amount of miR-21 generates numerous long ssDNAs. These long anionic ssDNAs are capable of absorbing abundant numbers of cationic MB molecules by electrostatic interactions (Castaño-Alvarez et al., 2009; García-González et al., 2014). When probed by an electrode at sufficient potential to cause redox changes in MB, a signal current is generated. The signal exhibits comparatively high sensitivity for label-free detection with a LOD of 3.04 aM. Herein, we describe how the PEDAR was skillfully introduced on the electrode surface, exhibiting better amplification efficiency. Additionally, the biosensor shows better discriminative performance even for a single base-mismatched target and the difference between tumorous miR-21 and non-tumorous miRNAs derived from exosomes. Overall, the proposed biosensor shows high sensitivity and selectivity and demonstrates promising clinical value for cancer detection.

2. Experimental sections

2.1. Materials

All HPLC-purified and lyophilized miRNAs and DNA oligonucleotides were purchased from Shanghai Sangon Biotech Co., Ltd. The corresponding sequences are shown in Table S1; their concentrations were measured by UV–Vis absorbance at 260 nm depended on their individual absorption coefficients. Bst DNA polymerase was purchased from New England Biolabs Co., Ltd. (Beijing, China). DATP, dTTP, dCTP and MB were purchased from Aladdin Biochemical Technology Co. Ltd. (Shanghai, China). All cells lines (Human breast cancer MCF-7 cell line, human mammary epithelial MCF-10A cell line, human cervical cancer HeLa cell line, and Chinese hamster ovary CHO–K1 cell line) were purchased from the China Center for Type Culture Collection in Shanghai. Fetal bovine serum (FBS), penicillin-streptomycin solution, Dulbecco's Modified Eagle Medium (DMEM) and Roswell Park Memorial Institute (RPMI) medium were purchased from Hyclone. The Mammary Epithelial Cell Growth Medium™ Bullet Kit-supplemented Mammary Epithelial Basal Medium (MEBM) was purchased from Lonza. ExoELISA-ULTRA CD63 kit was purchased from System Biosciences (SBI). Glutaraldehyde, paraformaldehyde, whole protein extraction kit and polyacrylamide gel electrophoresis (PAGE) DNA extraction kit were purchased from Beijing Solarbio Science & Technology Co., Ltd. Pierce™ Bicinchoninic Acid (BCA) Protein Assay Kit was purchased from Thermo Fisher Scientifc. Polyvinylidene fluoride membrane (PVDF) was purchased from Beijing Dingguo Changsheng Biotechnology Co., Ltd. CD63 antibody, TSG101 antibody and secondary antibody were purchased from Abcam. BeyoECL Moon (extremely super-sensitive chemiluminescence kit) was purchased from Beyotime Biotechnology Co., Ltd. The Exosome RNA Isolation Kit was purchased from Rengen Biosciences Co., Ltd (Liaoning, China). MiScript II RT Kit and miScript SYBR Green PCR Kit were purchased from Qiagen. All chemicals were of analytical grade. Milli-Q water (18.2 MΩ/cm) was used to prepare aqueous solutions in all experiments.

2.2. Exosomes isolation

MCF-7 cells and HeLa cells were cultured in DMEM containing 10% FBS, 1% penicillin and streptomycin. CHO–K1 cells were cultured in RPMI containing 10% FBS, 1% penicillin and streptomycin. MCF-10A cells were maintained in MEBM supplemented with 100 ng/mL cholera toxin. Then, various cells ($\sim 1.0 \times 10^8$ cells) were transferred to serum-free medium (Skog et al., 2008; Tosar et al., 2015) for 48 h followed by the collection of cell supernatant. Subsequently, exosomes were isolated from the cell supernatant by ultracentrifugation on Himac CS120FNX and CP100NX ultracentrifuges (Hitachi Ltd., Japan). According to previous work (Luo et al., 2020), the cell supernatant was centrifuged at 300 g, 2000 g and 11,000 g to remove the intact and dead cells, cell debris, and proteins, respectively. The cell supernatant was further centrifuged at 100,000 g to collect exosomal sediments. Finally, the exosomes were resuspended in sterile PBS and stored at −80 °C for later experiments. Exosomes isolation from human serum was obtained according to the reported protocol (Wang et al., 2017), with a slight modification in the following process: serum samples were first centrifuged at 11,000 g for 90 min. Subsequently, a 0.22 μm filter membrane was used to filter the supernatant. The filtered supernatant was centrifuged at 100,000 g for 70 min to collect the exosomes sediments. Lastly, the collected exosomes were resuspended in sterile PBS.

2.3. Exosomes characterization

2.3.1. Exosomes quantification by ExoELISA-ULTRA CD63 kit

Exosomes were quantified with the aid of a standard calibration curve (Figure S1) and measured using the ExoELISA-ULTRA CD63 kit. The following protocol was employed: 1) Exosomes samples were added to the microtiter plate and incubated at 37 °C for 1 h. 2) After three rinses, specific rabbit anti-human CD63 antibody was added and incubated for 1 h at room temperature. 3) The plate was incubated with HRP-conjugated goat anti-rabbit antibody for 1 h after washing. 4) After the final washing, the reaction was performed with super-sensitive 3, 3′, 5, 5′-Tetramethylbenzidine substrate followed by the addition of stop buffer. 5) The optical density was recorded at 450 nm using a the Epoch microplate spectrophotometer (BioTek Instruments Inc., U.S.A.).

2.3.2. Transmission electron microscopy (TEM)

Exosomes samples that had been mixed with equal-volumes of 4% paraformaldehyde were dropped on the surface of a copper mesh at room temperature for 20 min. The samples were fixed in 1% glutaraldehyde for 5 min, followed by washing with deionized water. Subsequently, excess water was blotted off with filter paper and the samples were stained with 1% uranyl acetate for 5 min. After drying in the air, the samples were imaged on a Tecnai G2 microscope (FEI, U.S.A.).

2.3.3. Dynamic light scattering (DLS)

According to previous work (Luo et al., 2020), the effective hydrodynamic diameters of exosomes were measured with a Litesizer 500 instrument (Anton Paar, Austria), equipped with a 35 mW laser diode source ($\lambda = 658$ nm). The scattered light was collected at an angle of 90°. One milliliter exosomes samples were suspended in filtered PBS and transferred to solvent-resistant cuvettes for light scatter measurements at the fixed position. The measurement temperature was maintained at room temperature.

2.3.4. Western blotting (WB)

The total proteins in cells and exosomes were extracted using the

whole protein extraction kit containing radio immunoprecipitation assay (RIPA) lysis buffer, and quantified by BCA assay. The proteins samples were mixed with loading buffer and denatured at 95 °C for 5 min. Then, the proteins samples were separated by 12% SDS-PAGE at 80 V for 30 min and 100 V for 90 min. Next, the proteins in gels were electrically transferred to pre-activated PVDF membranes in transfer buffer (25 mM Tris, 192 mM glycine, 20% methanol) at 300 mA for 15 min. After blocking with 5% non-fat powdered milk prepared in TBST (Tris buffered saline + Tween 20) buffer for 2 h, the PVDF membranes were incubated with CD63 antibody and TSG101 antibody at 4 °C overnight, respectively. Subsequently, the PVDF membranes were incubated with the secondary antibody at room temperature for 1 h. Finally, the immunoreactive bands were exposed to extremely super-sensitive chemiluminescence reagents and imaged using a Chem-iDoc™ Imaging System (Bio-Rad, U.S.A.).

2.4. RNA extraction and RT-PCR analysis of exosomes

Exosomal RNA was extracted using the exosome RNA Isolation Kit according to the protocol. Total RNA was quantified by a NanoDrop ND-2000 (Thermo Scientific) and converted to cDNA by miScript II RT Kit containing 5 × miScript HiSpec Buffer, 10 × miScript Nucleic Mix, RNase-free water and miScript Reverse Transcriptase Mix. The RT process was performed at 37 °C for 1 h and then inactivated by heating at 95 °C for 5 min. The PCR mixture was prepared using the miScript SYBR Green PCR Kit containing 2 × QuantiTect SYBR Green PCR Master Mix, 10 × miScript Universal Primer, 10 × miScript Primer Assay, and RNase-free water. The PCR assay was carried out on a Roche LightCycler® 96 (Roche, Switzerland) according to the recommended thermocycler protocol as follows: an initial activation step of 95 °C for 15 min and then 40 cycles of 94 °C for 15 s, 55 °C for 30 s, and 70 °C for 30 s. Finally, threshold cycle (Ct) data was collected with LightCycler 96 software.

2.5. Polyacrylamide gel electrophoresis

The TCSDR process was analyzed on 10% native PAGE gel. Initially, the two DNA probes consisting of the capture probes (Cp) and Pp were prepared in 1 × TAE (12.5 mM Mg^{2+}) and treated at 95 °C for 5 min. Subsequently, Cp was mixed with miR-21 and Pp at room temperature. The gel was run in 1 × TAE (12.5 mM Mg^{2+}) at 120 V for 110 min. Additionally, the products of PEDAR were verified on a 10% denaturing PAGE gel. The PEDAR reaction solution was first prepared by mixing the components of 10 mM dATP/dTTP/dCTP, 100 mM Mg^{2+}, 10 μM Tp, 1 μM dGTP-clean and 1200 U/mL Bst DNA polymerase, and then thermally incubated at 37 °C for 15 min. Before loading samples, the PEDAR reaction solution was incubated with Cp or Pp at 37 °C for 2 h. The gel was run in 1 × TBE at 120 V for 70 min. After electrophoresis on a Hoefer SE300 miniVE vertical electrophoresis system (Hoefer, Inc., U.S.A.), all gels were visualized with 0.1% Stains All, and scanned by scanner.

2.6. Electrode pretreatment and biosensor fabrication

The gold electrode (GE) was polished on a microcloth imbedded with 0.3 μm and 0.05 μm alumina powder, and ultrasonically cleaned with ethanol and Milli-Q water for 3 min each. After drying under a stream of nitrogen, the GE was immersed in H_2SO_4 and scanned by cyclic voltammetry (CV) until the CV curve was stable (Lao et al., 2005). CV was performed in the potential range from −0.35 V to +1.50 V, quiet time of 2 s, scan rate of 0.1 V/s, and sample interval of 0.001 V. The pretreated GE was then used to fabricate the electrochemical biosensor as follows. Initially, 3 μL of a 10 μM Cp solution prepared in 10 mM TE buffer containing 1 M NaCl, 10 mM trichloroethyl phosphate (TCEP), and 1 mM $MgCl_2$ was dropped on the surface of GE at room temperature for 30 min to form Cp/GE. After washing with water, Cp/GE was dipped in 5 mM mercaptohexanol (MCH) solution at 37 °C for 1.5 h to eliminate nonspecific adsorption of DNA. Then, the MCH/Cp/GE was incubated with miR-21 samples at room temperature for 45 min to form a miR-21/MCH/Cp/GE. Next, 3 μL of 2 μM Pp solution containing 2 mM $MgCl_2$ was spread on the surface of miR-21/MCH/Cp/GE and incubated at 37 °C for 45 min to replace and recycle miR-21, thus forming Pp/miR-21/MCH/Cp/GE (see Scheme 1). The above GE was incubated with premixed PEDAR reaction solution at 37 °C for 2 h. This was followed by incubation with MB. Finally, the fabricated GE was used for electrochemical detection.

2.7. Electrochemical detection

All electrochemical measurements were made with a conventional three-electrode system on a CHI660E electrochemical workstation (CH Instrument, Shanghai, China), consisting of a working electrode (GE with a diameter of 2 mm), a counter electrode (platinum wire) and a reference electrode (Ag/AgCl; 3 M KCl). CV and square wave voltammetry (SWV) were employed to analyze the electrochemical properties of the biosensor. CV was scanned with potential range from −0.5 V to +0.1 V, a quiet time of 2 s, scan rate of 0.1 V/s, and sample interval of 0.001 V. SWV was performed in the potential range from −0.5V to +0.1 V, potential step of 0.004 V, amplitude of 0.025 V, frequency of 15 Hz, and quiet time of 2 s.

3. Results and discussion

3.1. Experimental mechanism of the electrochemical biosensor

As shown in Scheme 1, numerous long ssDNAs produced by dual amplification reactions of TCSDR and PEDAR were incorporated in the electrochemical biosensor for the detection of exosomal miR-21. Initially, Cp was immobilized on GE through the Au–S bond, followed by the blocking reaction of MCH. In the presence of exosomal miR-21, miR-21 hybridizes with Cp, unfolding the hairpin structure of Cp and exposing the toehold that is complementary to Pp. Next, Pp binds to Cp and then displaces miR-21, allowing the displaced miR-21 to hybridize with other folded Cp. This step initiates the first amplification cycle of TCSDR. In theory, a single miR-21 molecule is capable of unfolding many hairpin structures of Cp, allowing multiple Pp to bind at unfolded Cp sites. Subsequently, the primer region a in Pp hybridizes with a* in the template probe Tp. This step initiates a second cascade process that carries out the second amplification reaction of PEDAR with the assistance of Bst DNA polymerase. In this process, primers are elongated along the stem region of Tp until the stop sequences appear. This reaction forms a copied region of a. Afterwards, the copied region a is displaced by the homologous region a in Tp through a branch strand migration reaction (Kishi et al., 2018; Lee et al., 1970). Tp then detaches from the extended DNA fragment aa. This is followed by the exposed a* in Tp hybridizing to copied region a for next new round of DNA amplification. N cycles later, primers can be seen in extended chains in the form of long ssDNAs (aaaa … a). In general, a single miR-21 molecule has the capacity to drive the generation of numerous long ssDNAs (aaaa … a) after undergoing two stages of amplification. These long ssDNAs absorb abundant quantities of MB and produce a strong signal from MB that is indicative of electrochemical oxidation. When miR-21 is absent, TCSDR and PEDAR do not execute and the electrochemical signal is small. The sensitive and selective detection of exosomal miR-21 will be demonstrated by measuring the current changes in the electrochemical signal before and after the addition of exosomal miR-21.

3.2. Feasibility characterization of dual amplification reactions

Before electrochemical sensing, PAGE was utilized to verify the feasibility of dual amplification reactions of TCSDR and PEDAR. First, the native PAGE analysis at different stages of TCSDR is shown in Fig. 1A. The bands in Lanes 1 and 2 belong to Cp and Pp, respectively. Lane 3 displays two bands. The upper band with a slow migration rate

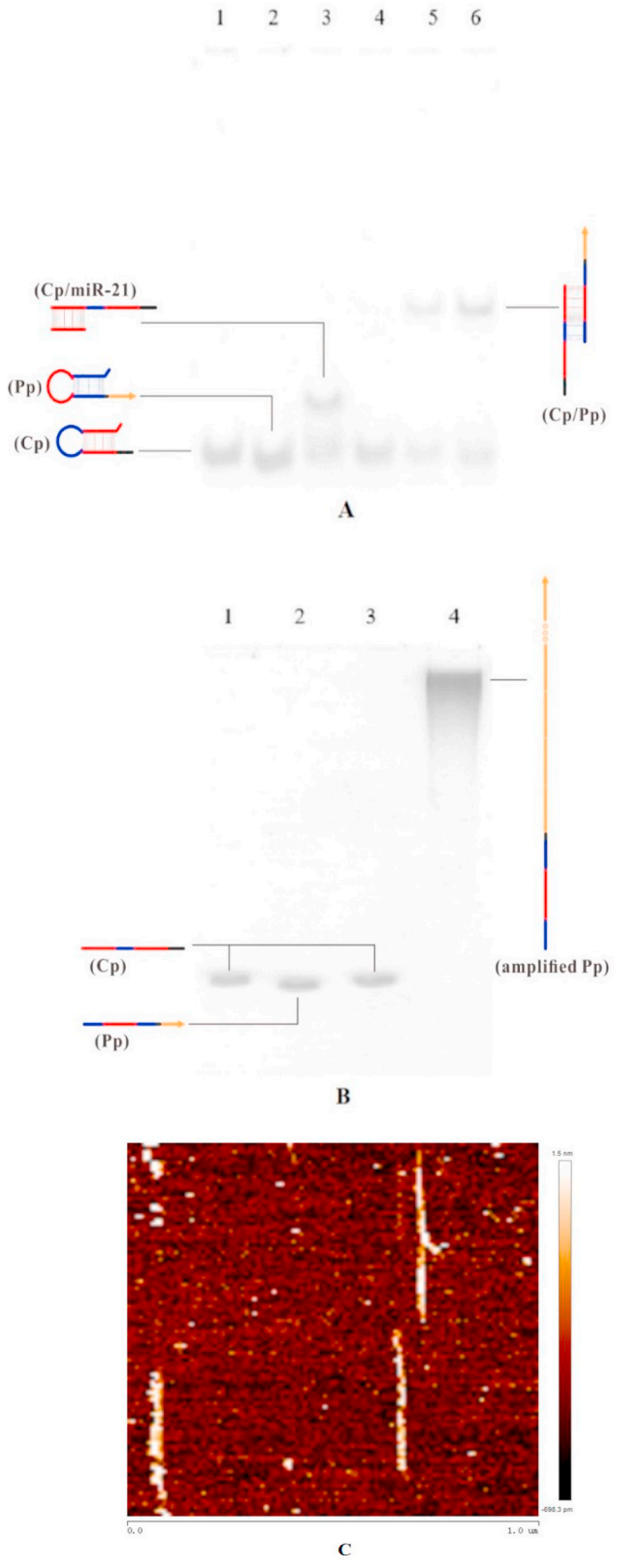

Fig. 1. (A)The native PAGE analysis of TCSDR. Lane 1: Cp; lane 2: Pp; lane 3: Cp + miR-21; lane 4: Cp (1 μM)+Pp (1 μM); lane 5: Cp (1 μM)+miR-21 (10 nM)+Pp (500 nM); lane 6: Cp (1 μM)+miR-21 (10 nM)+Pp (1 μM). (B). The denaturing PAGE analysis of PEDAR. Lane 1: Cp; lane 2: Pp; lane 3: the mixture of Cp and PEDAR solution; lane 4: the mixture of Pp and PEDAR solution. (C). The atomic force microscope imaging of long ssDNA purified by denaturing PAGE after the PEDAR process.

results from miR-21 hybridizing with Cp (Cp/miR-21). The faster migrating band is the remaining Cp. Lane 4 shows overlapping bands of Cp and Pp, indicating that Pp is unable to directly hybridize with the hairpin structure of Cp. In the confluent mixture of Cp (1 μM), miR-21 (10 nM) and Pp (500 nM) (Lane 5), however, a new band arises that is attributed to the double helix of Cp/Pp with a greater molecular weight and slower migration rate. This band suggests that Pp binds to unfolded Cp and replaces the miR-21 after miR-21 originally hybridized with Cp. After replacement, the displaced miR-21 is free to hybridize with other Cp probes. In Lane 6, the addition of more Pp (1 μM) allows continual reaction with Cp/miR-21, producing more Cp/Pp as it progresses. Thus, the band of Cp/Pp in Lane 6 is more intense than that in Lane 5, confirming the feasibility of TCSDR. Fig. 1B shows a denaturing PAGE analysis of the PEDAR. The bands in Lanes 1 and 2 arise from Cp and Pp, respectively (Cp and Pp in denaturing PAGE both exhibit single-stranded structures). The bands in Lanes 3 and 4 represent Cp and Pp, respectively, in the PEDAR reaction solution. The DNA band in Lane 3 is similar to that in Lane 1, indicating Cp unable to be amplified by PEDAR. In contrast, compared to the DNA band of Pp in Lane 2, a DNA band with an extremely large molecular weight emerges in Lane 4, and the band of single chain Pp disappears. These results demonstrate that Pp, by itself, is able to initiate the PEDAR process and synthetize long ssDNA. The long ssDNA purified by denaturing PAGE was retrieved using a PAGE DNA Extraction Kit, and imaged by an atomic force microscope (AFM). As shown in Fig. 1C, several long strip-like structures with a length range of 400–450 nm can be observed, which are similar to the reported AFM images of long ssDNA structures (Heenan and Perkins, 2019). The AFM imaging further indicates that the long ssDNA is successfully synthetized through PEDAR.

3.3. Feasibility characterization of the electrochemical biosensor

To validate the electrochemical measurements, CV and SWV were used to characterize different assembly processes on Au electrodes. As CV results in Fig. 2A shows, the redox peaks of MB in the potential range from −0.2 V to −0.3 V were negligible when MCH/GE (curve a) in buffer was measured. After Cp DNA was immobilized on GE (curve b), Cp DNA absorbs a small quantity of MB and produces a pair of small redox peaks in the potential range from −0.2 V to −0.3 V. Upon the addition of miR-21 (curve d) and then Pp (curve e), the adsorbed nucleic acids increases, resulting in a slight increase in peak current. After above assembled electrode is dipped in the PEDAR reaction solution (curve f), Pp triggers the amplification of PEDAR, generating a high yield of elongated ssDNAs. These ssDNAs absorb prolific amounts of MB, remarkably enhancing the current intensity under the redox peaks. In the absence of miR-21 (curve c), TCSDR and PEDAR failed to be initiated, and the redox peaks are small. SWV results are displayed in Fig. 2B. In the presence of miR-21, the current intensity under the oxidation peak in the potential range from −0.2 V to −0.3 V gradually and slightly increase before (curve a) and after the immobilization of Cp (curve b). The addition of miR-21 (curve d) and then Pp (curve e) produces progressively increasing oxidation peaks. Finally, the addition of Pp to the electrode in the presence of the PEDAR reaction solution (curve f) produces peaks of substantially greater intensity. By contrast, the oxidation peak of MB is small in the absence of miR-21 (curve c). The SWV results were consistent with that of CV which reveals it is feasible to use the electrochemical biosensor to detect miR-21. It is noteworthy that signal-to-background ratio (S/B) of the proposed electrochemical biosensor measured by SWV is greater than that measured by differential pulsed voltammetry (DPV) (Figure S2). Thus, the SWV measurement, a rapid and effective electro-analytical technique more sensitive than CV or DPV (Uslu et al., 2005, 2006), was used to evaluate the performance of this biosensor. We also checked our measurements using an AFM characterization of different assembled electrodes. As shown in Fig. S3, in the presence of miR-21 (Figure S3A), the height of the electrode surface after the reactions of TCSDR and PEDAR is distinctly higher than that in

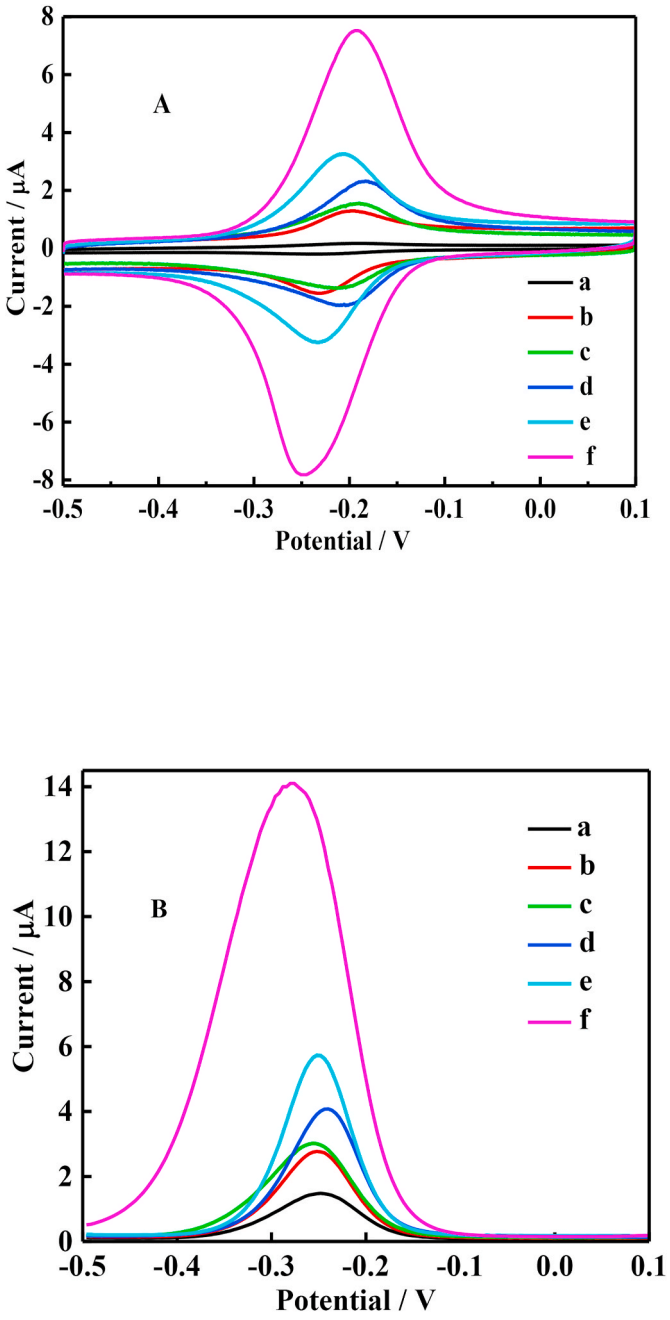

Fig. 2. The CV curves (A) and SWV curves (B) of different assembly electrodes in PBS buffer. a. MCH/GE; b: MCH/Cp/GE; c. PEDAR/Pp/MCH/Cp/GE; d. miR-21/MCH/Cp/GE; e. Pp/miR-21/MCH/Cp/GE; f. PEDAR/Pp/miR-21/MCH/Cp/GE.

the absence of miR-21 (Figure S3B).

3.4. Optimizations of experimental conditions

Before applying the biosensor to detect exosomal miR-21, we optimized the performance of this biosensor by investigating the experimental conditions which affects the current change (ΔI) before and after the addition of miR-21. We first considered how different concentrations of Cp influence the TCSDR process. As depicted in Figure S4A, ΔI achieves its best value when the concentration of Cp is set to 10 μM. At this value, the density of Cp on the electrode was quantified by chronocoulometry (Figure S5), according to the literatures (Lao et al., 2005; Steel et al., 1998); it was calculated to be ~3.40×10^{11} molecules/cm^2. To investigate the reproducibility of the immobilization of Cp on the electrode surface, identical and different batches of electrodes were used in 5 separate experiments. We obtained the relative standard deviation (RSD) of intra- and inter-assay of 3.16% and 4.63% (Table S2), respectively. The above results indicate the extent to which reproducible quantities of Cp were immobilized on the electrode surfaces. As shown in Figure S4B, C, D, E, the conditions found optimal to conduct the TCSDR process required 30 min Cp immobilization time, 1 mM Mg^{2+} in the Cp buffer, 2 μM Pp concentration, and 45 min Pp reaction time. Finally, the parameters influencing the reaction of PEDAR, including the concentration of Bst DNA polymerase (C_{Bst}), as well as the Tp concentration (C_{Tp}) and the PEDAR reaction time, were also measured. As shown in Figure S6, the optimized C_{Bst}, C_{Tp} and PEDAR reaction time are 1200 U/mL, 10 μM and 120 min, respectively.

3.5. The detection performance of the electrochemical biosensor

On the basis of the above optimized conditions, we investigated the performance (e.g., sensitivity, selectivity, stability and reproducibility) of the electrochemical biosensor using SWV. The dynamic range and sensitivity of this biosensor were first analyzed. As shown in Fig. 3A, the current signal gradually increases with the increasing of miR-21 concentration from 0 to 10^7 aM. The current changes (ΔI) before and after adding different concentrations of miR-21 (C_{miR-21}) were recorded and evaluated. Over the wide dynamic range from 10 aM to 10^7 aM, which spans 7 orders of magnitude, the calibration curve in Fig. 3A inset shows a good linear relationship between ΔI and the logarithm of C_{miR-21} ($logC_{miR-21}$). The associated linear regression equation is $\Delta I = 1.4602 (logC_{miR-21}) - 0.2565$. The correlation coefficient (r) is 0.9983. Based on the 3σ (σ is the standard deviation of the background signal) rule (Qian et al., 2015), the LOD was calculated to be 3.04 aM by substituting 3σ (σ = 0.1495) in the linear regression equation as ΔI for the calculation of C_{miR-21} (C_{miR-21} was the LOD). We note that high sensitivity was achieved through the dual amplification reactions of TCSDR and PEDAR occurring simultaneously.

To determine the discrimination and selectivity of the electrochemical biosensor, we challenged the dual amplification assay with different mismatched miRNAs and homologous miRNAs. The miRNAs are inclusive of miR-21, and also contain single-, double- and three-base mismatches in miR-21 sequence, plus non-complementary sequences, as well as several extraneous miRNAs of miR-122, miR-155, miR-144, miR-199a, let-7a and let-7g. Several of these have high homology to miR-21 (Cao et al., 2019; Kangkamano et al., 2018; Zhu et al., 2016). As shown in Fig. 3B, the perfectly matched miR-21 produced a current change (ΔI) at least 9.5 times greater than other mismatched sequences and homologous miRNAs. This result shows that the biosensor exhibits selective recognition of miR-21 and is able to differentiate it from other sequences with high similarity, even to the limit of single-base mismatch.

To monitor the stability of the biosensor over time, we stored the fabricated biosensors in PBS at 4 °C for 7 days and tested their responses. As shown in Figure S7A, the current change after 7 days were maintained to within 96.74% of the original signal. Meanwhile, the biosensor was challenged with miR-21-spiked human serum in a separate series of experiments. Figure S7B shows the current changes vary from 98.08% to 101.60% of the no serum values after incubating the biosensor with 50% human serum spiked with miR-21 at different concentrations. Additionally, the detection of 1 fM and 10 pM miR-21 was repeated under identical conditions for 5 times to assess the reproducibility of the biosensor. As shown in Table S3, the RSD from the mean values were 3.16% and 2.56% for 1 fM and 10 pM spiked targets.

Overall, compared to most of recently reported biosensors (Table 1), the proposed electrochemical biosensor has generally better sensitivity and selectivity, all the while maintaining good stability and reproducibility. Some fluorescent and electrochemical biosensors report somewhat better discrimination between the signals produced by the target

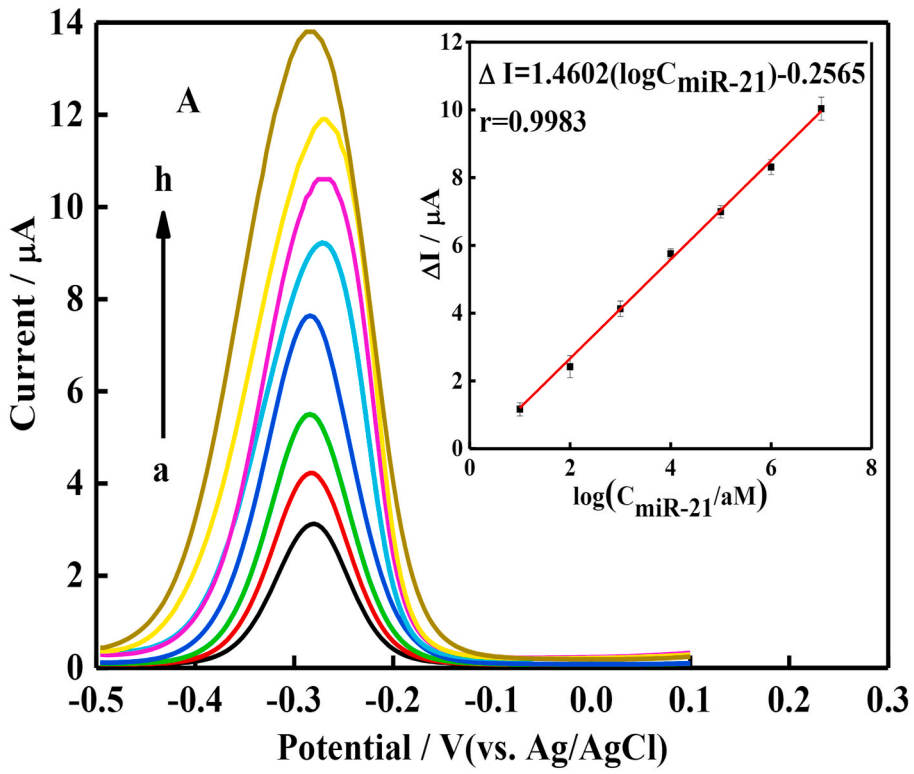

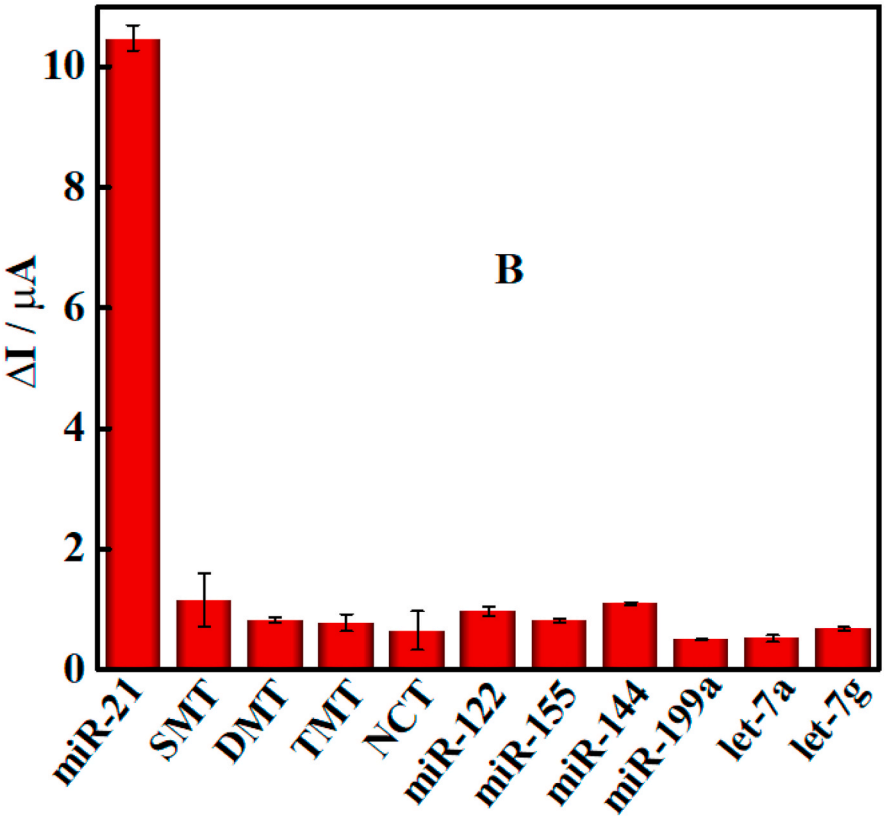

Fig. 3. The sensitivity analysis of proposed electrochemical biosensor. (A). The current signals of different concentrations of miR-21 on the biosensor. MiR-21 concentrations (from a to h, in aM): 0, 10, 10^2, 10^3, 10^4, 10^5, 10^6, 10^7. Inset: the calibration curve fitted by the current change (ΔI) before and after the addition of miR-21 and the logarithm of C_{miR-21} ($logC_{miR-21}$). Error bars represent the standard deviations for measurements taken from three independent experiments. (B). The selectivity analysis of the proposed biosensor towards miR-21, mismatched miR-21 (SMT: single base mismatched target; DMT: double bases mismatched target; TMT: three bases mismatched target; NCT: non-complementary target) and homologous miRNAs (miR-122, miR-155, miR-144, miR-199a, let-7a and let-7g) at the same concentration of 10^7 aM. Error bars represent standard deviations for measurements taken from three independent experiments.

Table 1
Different biosensors for detection of exosomal miRNAs in recent years.
* Selectivity was analyzed by the ratio of the signals produced by target and the mismatched target or homologous miRNAs.

Methods	LOD	Selectivity*	Stability	Reproducibility (RSD %)	Refs.
Dual-SERS biosensor	1 aM	>2	Good (4 °C for 90 days)	3.03%	Pang et al. (2019)
Surface-enhanced Raman scattering sensor	1 aM	>2.5	N/A	4.53%	Lee et al., 2019b
Surface plasmon resonance biosensor	0.2 fM; 10 fM; 40 pM	>7.5	Good (50% human serum and plasma)	N/A	Zou et al., 2020
Fluorescence biosensor	90 fM	>1.5	N/A	N/A	Wang et al., 2020b
Thermophoretic detection	0.36 fM	N/A	N/A	N/A	Zhao et al. (2020)
Multiplex fluorescence biosensor	462 pM; 154 pM; 301 pM	>6	Good (cell culture medium and FBS serum)	0.96%	Wang et al., 2020a
Fluorescence biosensor	1.5 fM	>10	N/A	N/A	Wang et al., 2019b
Ratiometric electrochemical DNA biosensor	2.3 fM	>50	N/A	2.15%	Luo et al. (2020)
Ratiometric electrochemical biosensor	67 aM	>10	N/A	3.21–4.47%	Zhang et al. (2018)
Electrochemical biosensor	49 aM	>3.5	Good (10% human serum)	<5.0%	Liu et al. (2019)
Electrochemical biosensor	2.75 fM	>2	Good (4 °C for 7 days, 100.26% signal; 14 days, 100.26% signal; 21 days, 78.01% signal	9.81%	Tang et al. (2020)
Electrochemical biosensor	53 aM	>7	N/A	2.69–3.46%	Guo et al. (2020)
Electrochemical biosensor	0.4 fM	>10	N/A	N/A	Cheng et al., 2020
Electrochemical biosensor	7.3 aM	>10	Good (serum conditions, 96.4%–106.0% signal)	2.9–4.9%	Miao and Tang (2020)
Electrochemical biosensor	100 aM	>7	N/A	<5.0%	Masud et al., 2020
Electrochemical biosensor	3.04 aM	>9.5	Good (4 °C for 7 days, 96.74% signal; 50% human serum, 98.08%–101.60% signal)	2.56–3.16%	This work

and the mismatched or homologous miRNAs. The sensitivity or stability of these biosensors should be further investigated for additional improvement. Although some biosensors based on SERS have lower LOD, their expensive and large apparatus as well as their complicated operation may limit their acceptance. In this work, the electrochemical biosensor with good performance possesses the benefits of low cost, easy operation, and portability, all of which enhance the potential benefit in the development of point-of-care testing (POCT).

3.6. Detection of exosomal miR-21 derived from cells and serum samples

To evaluate practical clinical applications, we employed the proposed electrochemical biosensor to detect endogenous miR-21 found within the total exosomal RNA extracted from breast cancer MCF-7 cells. Exosomes were collected by ultracentrifugation and characterized by TEM, DLS and WB. As shown in Fig. 4A, TEM image (inset) and DLS result demonstrate that MCF-7 cells-derived exosomes have a cup or saucer-like vesicle structure with a diameter range between 75 and 115 nm. The WB results in Figure S8 show apparent bands belonging to the CD63 and TSG101 proteins of MCF-7 cells-derived exosomes can be observed. In addition, the TEM image (Figure S9A), DLS result (Figure S9B) and WB results (Figure S9C) of exosomes derived from MCF-10A cells as contrast examples were characterized. The above characterizations for the morphology, size and proteins of exosomes are consistent with previous reports (Liu et al., 2019; Wang et al., 2019a). Afterwards, 6.8×10^{11} exosomes (quantified by standard curve in Figure S1) derived from MCF-7 cells were isolated to extract total RNA. The expression level of MCF-7 cells-derived exosomal miR-21 in total RNA was analyzed by determining the Ct value through RT-PCR. As shown in Fig. 4B, the Ct values of exosomal miR-21 and the internal control of U6 snRNA were 28.63 and 31.65, respectively. The results conformed with those previously reported (Luo et al., 2020; Wickramasinghe et al., 2009). In addition, the proposed electrochemical biosensor was used to detect exosomal miR-21 levels in MCF-7 cells and MCF-10A cells. As shown in Fig. 4C, the detection level of exsomal miR-21 extracted from human breast cancer cells (MCF-7) is discernably greater than that extracted from human mammary epithelial cells (MCF-10A). Meanwhile, the levels of exosomal miR-21 in other tumor cells (HeLa) and non-tumorous cells (CHO–K1) were also detected as a comparison. The morphology and sizes of exosomes from HeLa cells and CHO–K1 cells were also characterized using TEM and DLS (Figure S10). As shown in Figure S11, exosomal miR-21 extracted from MCF-7 cells are measured at higher level that can be well distinguished from that taken from HeLa cells and CHO–K1 cells, indicating the relative overexpression of exosomal miR-21 in MCF-7 cells compared to HeLa cells (Liu et al., 2019) and CHO–K1 cells (Lee et al., 2015). The above electrochemical results are in accord with those obtained by the PCR method.

We also employed the electrochemical biosensor to measure the concentrations of exosomal miR-21 from clinical serum samples of breast cancer patients and normal controls. According to the relevant guidelines and regulations, 6 breast cancer patient serum samples and 6 normal control serum samples were collected. The exosomes collection and RNA extraction procedures were carried out according to the protocols outlined in section 2.2 and 2.4. As shown in Fig. 4D, the exosomal miR-21 levels in serum samples from breast cancer patients are notably higher than that of the normal controls ($P < 0.0001$), which is confirmed by the results obtained using the PCR method. The above results indicate that the exosomal miR-21 in breast cancer patients is up-regulated compared to levels found in normal people (Liu et al., 2019; Zhang et al., 2018). We interpret these results as verifying the usefulness of exosomal miR-21 as an important cancer biomarker. It also validates the potential practical value of using this biosensor for miRNAs analysis, with special emphasis on early cancer screening and diagnosis.

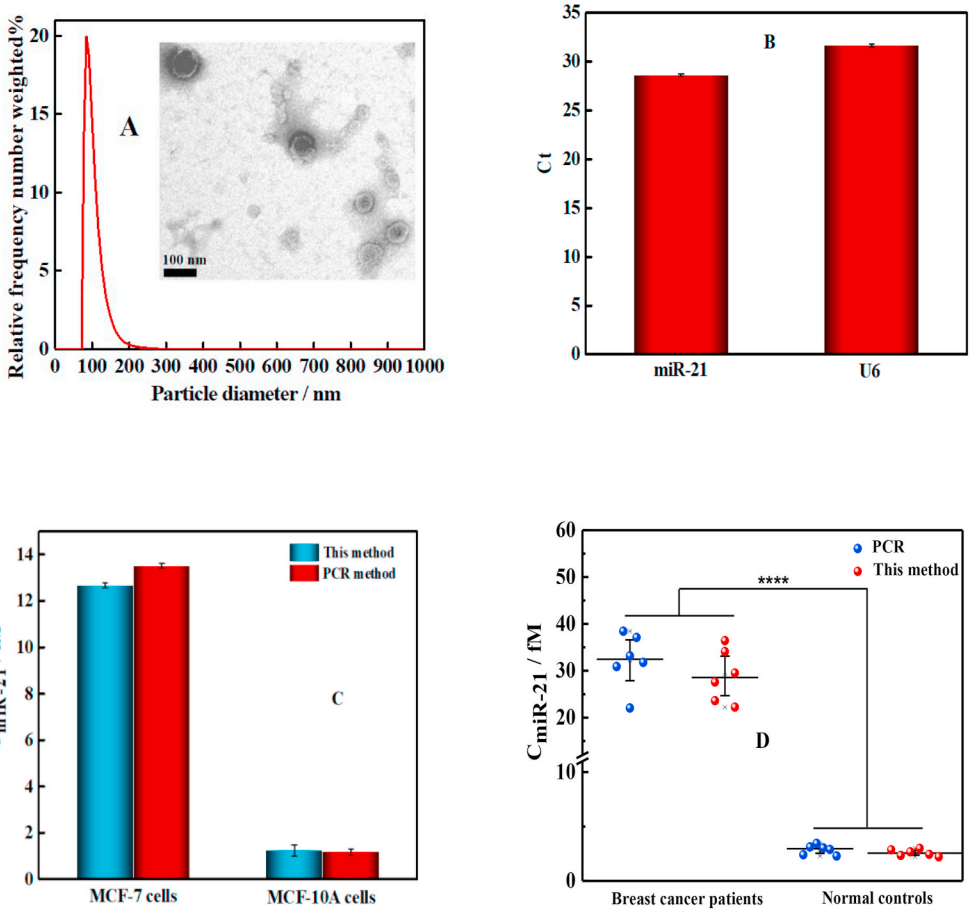

Fig. 4. (A). The DLS result of MCF-7 cells-derived exosomes. Inset: The TEM imaging of MCF-7 cells-derived exosomes. (B). Ct values of exosomal miR-21 and U6 snRNA derived from MCF-7 cells. (C). Measurements of exsomal miR-21 from MCF-7 cells and MCF-10A cells by the electrochemical biosensor and PCR method. The same amount of exosomes from each cell were used for miR-21 analysis for comparison. (D). The detection of exosomal miR-21 in serum samples from breast cancer patients and normal controls using the PCR method and the electrochemical biosensor. ****P < 0.0001 (Two-tailed *t*-test).

4. Conclusion

In summary, a label-free electrochemical biosensor for the detection of exosomal miRNAs was developed based on numerous long single-stranded DNAs produced by dual amplification reactions of TCSDR and PEDAR. The electrochemical biosensor shows the following features. 1) The combination of dual amplification reactions leads to highly sensitive detection with a LOD as low as 3.04 aM. TCSDR acts as a catalytic propeller for initiating PEDAR amplification in the presence of numerous primers, the combination producing high amplification efficiency. 2) PEDAR occurs at the electrochemical interface to detect exosomal miRNAs. This feature has the advantage of enabling automated and programmable one step amplification. 3) In this biosensor, PEDAR can be directly and easily generalized for accommodating the detection of a diverse number of miRNAs by changing the capture probe sequence and its complementary DNA probe. 4) The electrochemical biosensor touts intrinsic benefits of simple operation, low cost, and high selectivity to the level of discriminating a single base variation in target miRNAs. Its portability lends this instrumentation to the development of POCT (Jin et al., 2020). In future work, a split-probe strategy (Choi et al., 2018) and binary hairpin probes (Marras et al., 2019) for miRNAs binding will be introduced to further reduce the possibly of non-specific binding in the target binding process. In addition, nano-architecture frameworks (Masud et al., 2019) and anti-fouling materials (Sabaté Del Río et al., 2019) will be introduced to improve the performance of the electrochemical sensing interface. Overall, the proposed electrochemical biosensor demonstrates significant potential for detecting exosomal miRNAs in real samples as well as for use in early tumor diagnosis and screening.

CRediT authorship contribution statement

Liang-Liang Wang: Conceptualization, Validation, Writing - original draft, Methodology. **Wen-Qian Chen:** Methodology, Investigation. **Yu-Ru Wang:** Investigation, Visualization. **Lu-Peng Zeng:** Formal analysis. **Ting-Ting Chen:** Formal analysis. **Guan-Yu Chen:** Data curation. **Jing-Hua Chen:** Resources, Writing - review & editing, Funding acquisition, Supervision.

Declaration of competing interest

The authors declare that they have no known competing financial interests or personal relationships that could have appeared to influence the work reported in this paper.

Acknowledgement

The authors gratefully acknowledge the financial support of National Natural Science Foundation of China (Nos. 21874019), Young Top-notch Talent Project of Colleges and Universities of Fujian Province (3002360301), Natural Science Foundation of Fujian Province (Nos. 2017J07001), Startup Fund for Scientific Re-search, Fujian Medical University (2018QH2015).

Appendix A. Supplementary data

Supplementary data to this article can be found online at https://doi.org/10.1016/j.bios.2020.112555.

References

Abolhasan, R., Mehdizadeh, A., Rashidi, M.R., Aghebati-Maleki, L., Yousefi, M., 2019. Biosens. Bioelectron. 129, 164–174.

Aghebati-Maleki, A., Nami, S., Baghbanzadeh, A., Karzar, B.H., Noorolyai, S., Fotouhi, A., Aghebati-Maleki, L., 2019. J. Cell. Physiol. 234, 21694–21706.

Amorim, M.G., Valieris, R., Drummond, R.D., Pizzi, M.P., Freitas, V.M., Sinigaglia-Coimbra, R., Calin, G.A., Pasqualini, R., Arap, W., Silva, I.T., Dias-Neto, E., Nunes, D. N., 2017. Sci. Rep. 7, 14395.

Boriachek, K., Islam, M.N., Möller, A., Salomon, C., Nguyen, N.T., Hossain, M.S.A., Yamauchi, Y., Shiddiky, M.J.A., 2018a. Small 14, 1702153.

Boriachek, K., Umer, M., Islam, M.N., Gopalan, V., Lam, A.K., Nguyen, N.T., Shiddiky, M. J.A., 2018b. Analyst 143, 1662–1669.

Cao, H., Zhou, X., Zeng, Y., 2019. Sensor. Actuator. B Chem. 279, 447–457.

Castaño-Alvarez, M., Fernández-la-Villa, A., Fernández-Abedul, M.T., Costa-García, A., 2009. Electrophoresis 30, 1943–1948.

Cheng, W., Ma, J., Cao, P., Zhang, Y., Xu, C., Yi, Y., Li, J., 2020. Talanta 219, 121242.

Cho, S., Yang, H.C., Rhee, W.J., 2019. Biosens. Bioelectron. 146, 111749.

Choi, J.R., Hu, J., Tang, R., Gong, Y., Feng, S., Ren, H., Wen, T., Li, X., Wan Abas, W.A., Pingguan-Murphy, B., Xu, F., 2016. Lab Chip 16, 611–621.

Choi, H.M.T., Schwarzkopf, M., Fornace, M.E., Acharya, A., Artavanis, G., Stegmaier, J., Cunha, A., Pierce, N.A., 2018. Development 145, dev165753.

Dai, Y., Liu, C.C., 2019. Angew Chem. Int. Ed. Engl. 58, 12355–12368.

Fong, M.Y., Zhou, W., Liu, L., Alontaga, A.Y., Chandra, M., Ashby, J., Chow, A., O'Connor, S.T., Li, S., Chin, A.R., Somlo, G., Palomares, M., Li, Z., Tremblay, J.R., Tsuyada, A., Sun, G., Reid, M.A., Wu, X., Swiderski, P., Ren, X., Shi, Y., Kong, M., Zhong, W., Chen, Y., Wang, S.E., 2015. Nat. Cell Biol. 17, 183–194.

Gao, X., Li, S., Ding, F., Fan, H., Shi, L., Zhu, L., Feng, J., Zhu, X., Zhang, C., 2019. Angew Chem. Int. Ed. Engl. 58, 8719–8723.

García-González, R., Costa-García, A., Fernández-Abedul, M.T., 2014. Sensor. Actuator. B Chem. 191, 784–790.

Groza, M., Zimta, A.A., Irimie, A., Achimas-Cadariu, P., Cenariu, D., Stanta, G., Berindan-Neagoe, I., 2020. J. Cell. Physiol. 235, 691–705.

Guo, Q., Yu, Y., Zhang, H., Cai, C., Shen, Q., 2020. Anal. Chem. 92, 5302–5310.

Hannafon, B.N., Trigoso, Y.D., Calloway, C.L., Zhao, Y.D., Lum, D.H., Welm, A.L., Zhao, Z.J., Blick, K.E., Dooley, W.C., Ding, W.Q., 2016. Breast Cancer Res. 18, 90.

He, Y., Deng, F., Yang, S., Wang, D., Chen, X., Zhong, S., Zhao, J., Tang, J., 2018. Biomarkers Med. 12, 177–188.

Heenan, P.R., Perkins, T.T., 2019. ACS Nano 13, 4220–4229.

Hou, T., Li, W., Liu, X., Li, F., 2015. Anal. Chem. 87, 11368–11374.

Jiang, L., Gu, Y., Du, Y., Liu, J., 2019. Mol. Pharm. 16, 3333–3349.

Jin, X., Liu, C., Xu, T., Su, L., Zhang, X., 2020. Biosens. Bioelectron. 165, 112412.

Kalluri, R., LeBleu, V.S., 2020. Science 367, eaau6977.

Kangkamano, T., Numnuam, A., Limbut, W., Kanatharana, P., Vilaivan, T., Thavarungkul, P., 2018. Biosens. Bioelectron. 102, 217–225.

Kishi, J.Y., Schaus, T.E., Gopalkrishnan, N., Xuan, F., Yin, P., 2018. Nat. Chem. 10, 155–164.

Kishi, J.Y., Lapan, S.W., Beliveau, B.J., West, E.R., Zhu, A., Sasaki, H.M., Saka, S.K., Wang, Y., Cepko, C.L., Yin, P., 2019. Nat. Methods 16, 533–544.

Kulkarni, B., Kirave, P., Gondaliya, P., Jash, K., Jain, A., Tekade, R.K., Kalia, K., 2019. Drug discov. Today Off. 24, 2058–2067.

Lao, R., Song, S., Wu, H., Wang, L., Zhang, Z., He, L., Fan, C., 2005. Anal. Chem. 77, 6475–6480.

Lee, J.H., Choi, J.H., Chueng, S.D., Pongkulapa, T., Yang, L., Cho, H.Y., Choi, J.W., Lee, K.B., 2019a. ACS Nano 13, 8793–8803.

Lee, C.S., Davis, R.W., Davidson, N., 1970. J. Mol. Biol. 48, 1–22.

Lee, J.H., Kim, J.A., Kwon, M.H., Kang, J.Y., Rhee, W.J., 2015. Biomaterials 54, 116–125.

Lee, J.U., Kim, W.H., Lee, H.S., Park, K.H., Sim, S.J., 2019b. Small 15, e1804968.

Liu, L., Lu, H., Shi, R., Peng, X.X., Xiang, Q., Wang, B., Wan, Q.Q., Sun, Y., Yang, F., Zhang, G.J., 2019. Anal. Chem. 91, 13198–13205.

Luo, L., Wang, L., Zeng, L., Wang, Y., Weng, Y., Liao, Y., Chen, T., Xia, Y., Zhang, J., Chen, J., 2020. Talanta 207, 120298.

Marras, S.A.E., Bushkin, Y., Tyagi, S., 2019. Proc. Natl. Acad. Sci. U. S. A 116, 13921–13926.

Masud, M.K., Mahmudunnabi, R.G., Aziz, N.B., Stevens, C.H., Do-Ha, D., Yang, S., Blair, I.P., Hossain, M.S.A., Shim, Y.B., Ooi, L., Yamauchi, Y., Shiddiky, M.J.A., 2020. ChemElectroChem 7, 3459–3467.

Masud, M.K., Umer, M., Hossain, M.S.A., Yamauchi, Y., Nguyen, N.T., Shiddiky, M.J.A., 2019. Trends Biochem. Sci. 44, 433–452.

Miao, P., Tang, Y., 2020. Anal. Chem. 92, 12026–12032.

Pan, D., Zuo, X., Wan, Y., Wang, L., Zhang, J., Song, S., Fan, C., 2007. Sensors 7, 2671–2680.

Pang, Y., Wang, C., Lu, L., Wang, C., Sun, Z., Xiao, R., 2019. Biosens. Bioelectron. 130, 204–213.

Qian, Y., Wang, C., Gao, F., 2015. Biosens. Bioelectron. 63, 425–431.

Qu, L., Ding, J., Chen, C., Wu, Z.J., Liu, B., Gao, Y., Chen, W., Liu, F., Sun, W., Li, X.F., Wang, X., Wang, Y., Xu, Z.Y., Gao, L., Yang, Q., Xu, B., Li, Y.M., Fang, Z.Y., Xu, Z.P., Bao, Y., Wu, D.S., Miao, X., Sun, H.Y., Sun, Y.H., Wang, H.Y., Wang, L.H., 2016. Canc. Cell 29, 653–668.

Sabaté Del Río, J., Henry, O.Y.F., Jolly, P., Ingber, D.E., 2019. Nat. Nanotechnol. 14, 1143–1149.

Saka, S.K., Wang, Y., Kishi, J.Y., Zhu, A., Zeng, Y., Xie, W., Kirli, K., Yapp, C., Cicconet, M., Beliveau, B.J., Lapan, S.W., Yin, S., Lin, M., Boyden, E.S., Kaeser, P.S., Pihan, G., Church, G.M., Yin, P., 2019. Nat. Biotechnol. 37, 1080–1090.

Salehi, M., Sharifi, M., 2018. J. Cell. Physiol. 233, 6370–6380.

Skog, J., Würdinger, T., van Rijn, S., Meijer, D.H., Gainche, L., Sena-Esteves, M., Curry Jr., W.T., Carter, B.S., Krichevsky, A.M., Breakefield, X.O., 2008. Nat. Cell Biol. 10, 1470–1476.

Steel, A.B., Herne, T.M., Tarlov, M.J., 1998. Anal. Chem. 70, 4670–4677.

Tang, X., Wang, Y., Zhou, L., Zhang, W., Yang, S., Yu, L., Zhao, S., Chang, K., Chen, M., 2020. Mikrochim. Acta 187, 172.

Tavallaie, R., McCarroll, J., Le Grand, M., Ariotti, N., Schuhmann, W., Bakker, E., Tilley, R.D., Hibbert, D.B., Kavallaris, M., Gooding, J.J., 2018. Nat. Nanotechnol. 13, 1066–1071.

Tosar, J.P., Gámbaro, F., Sanguinetti, J., Bonilla, B., Witwer, K.W., Cayota, A., 2015. Nucleic Acids Res. 43, 5601–5616.

Uslu, B., Dogan, B., Ozkan, S.A., 2005. Anal. Chim. Acta 537, 307–313.

Uslu, B., Ozkan, S.A., Senturk, Z., 2006. Anal. Chim. Acta 555, 341–347.

Valadi, H., Ekström, K., Bossios, A., Sjöstrand, M., Lee, J.J., Lötvall, J.O., 2007. Nat. Cell Biol. 9, 654–659.

Wang, H.X., Gires, O., 2019. Canc. Lett. 460, 54–64.

Wang, H., He, D., Wan, K., Sheng, X., Cheng, H., Huang, J., Zhou, X., He, X., Wang, K., 2020a. Analyst 145, 3289–3296.

Wang, Y.M., Liu, J.W., Adkins, G.B., Shen, W., Trinh, M.P., Duan, L.Y., Jiang, J.H., Zhong, W., 2017. Anal. Chem. 89, 12327–12333.

Wang, Y., Luo, D., Fang, Y., Wu, W., Wang, Y., Xia, Y., Wu, F., Li, C., Lan, J., Chen, J., 2019a. Sensor. Actuator. B Chem. 298, 126900.

Wang, B., You, Z., Ren, D., 2019b. Analyst 144, 2304–2311.

Wang, R., Zhao, X., Chen, X., Qiu, X., Qing, G., Zhang, H., Zhang, L., Hu, X., He, Z., Zhong, D., Wang, Y., Luo, Y., 2020b. Anal. Chem. 92, 2176–2185.

Wickramasinghe, N.S., Manavalan, T.T., Dougherty, S.M., Riggs, K.A., Li, Y., Klinge, C. M., 2009. Nucleic Acids Res. 37, 2584–2595.

Yoshii, S., Hayashi, Y., Iijima, H., Inoue, T., Kimura, K., Sakatani, A., Nagai, K., Fujinaga, T., Hiyama, S., Kodama, T., Shinzaki, S., Tsujii, Y., Watabe, K., Takehara, T., 2019. Canc. Sci. 110, 2396–2407.

Zeng, Z., Li, Y., Pan, Y., Lan, X., Song, F., Sun, J., Zhou, K., Liu, X., Ren, X., Wang, F., Hu, J., Zhu, X., Yang, W., Liao, W., Li, G., Ding, Y., Liang, L., 2018. Nat. Commun. 9, 5395.

Zhang, W., Xia, W., Lv, Z., Ni, C., Xin, Y., Yang, L., 2017. Cell. Physiol. Biochem. 41, 755–768.

Zhang, J., Wang, L.L., Hou, M.F., Xia, Y.K., He, W.H., Yan, A., Weng, Y.P., Zeng, L.P., Chen, J.H., 2018. Biosens. Bioelectron. 102, 33–40.

Zhao, Y., Chen, F., Li, Q., Wang, L., Fan, C., 2015. Chem. Rev. 115, 12491–12545.

Zhao, J., Liu, C., Li, Y., Ma, Y., Deng, J., Li, L., Sun, J., 2020. J. Am. Chem. Soc. 142, 4996–5001.

Zhu, Y., Qiu, D., Yang, G., Wang, M., Zhang, Q., Wang, P., Ming, H., Zhang, D., Yu, Y., Zou, G., Badugu, R., Lakowicz, J.R., 2016. Biosens. Bioelectron. 85, 198–204.

Zou, L., Wu, Z., Liu, X., Zheng, Y., Mei, W., Wang, Q., Yang, X., Wang, K., 2020. Anal Chem. 92, 11953–11959.